Modeling energy-loss spectra due to phonon excitation

B. D. Forbes and L. J. Allen*
School of Physics, University of Melbourne, Parkville, Victoria 3010, Australia
(Received 23 March 2016; revised manuscript received 11 May 2016; published 13 July 2016)

We discuss a fundamental theory of how to calculate the phonon-loss sector of the energy-loss spectrum for electrons scattering from crystalline solids. A correlated model for the atomic motion is used for calculating the vibrational modes. Spectra are calculated for crystalline silicon illuminated by a plane wave and by an atomic-scale focused coherent probe, in which case the spectra depend on probe position. These spectra are also affected by the size of the spectrometer aperture. The correlated model is contrasted with the Einstein model in which atoms in the specimen are assumed to vibrate independently. We also discuss how both the correlated and Einstein models relate to a classical view of the energy-loss process.

DOI: 10.1103/PhysRevB.94.014110

I. INTRODUCTION

In electron energy-loss spectroscopy (EELS) on a specimen of condensed matter, the region below approximately 100 eV is often referred to as the low-loss region of the spectrum. Interband electronic transitions contribute to this region and are often superimposed on plasmon peaks, which are present at similar energies. In the context of transmission electron microscopy, monochromators and spectrometers with a resolution of the order of 10 meV allow such overlapping peaks to be resolved and details in energy-loss spectra can also be observed closer to the zero energy loss, meaning that band gaps and vibrational spectra associated with phonon excitation are accessible [1]. An atomic-scale focused coherent probe in scanning transmission electron microscopy (STEM) allows information to be obtained from nanometer-sized regions, making it possible, in principle, to detect localized vibrational excitations. The phonon-loss sector is of potential importance in materials studies since it will allow detailed studies of interfaces, defects, bonding arrangements, and the detection of hydrogen and other light elements [1].

Excitation of optical surface phonons by electrons in zinc oxide was observed more than four decades ago [2] and an electron-spectroscopic study of amorphous germanium and silicon in the two-phonon region was reported shortly thereafter [3]. With the ability to measure localized phonon spectra in STEM, there have been several recent explorations of the possibilities that this offers as well as the pertinent experimental factors [1,4–7]. The subtraction of the zero-loss peak is a major issue, with both Egerton and Rez pointing out that, given the small magnitude of the scattering cross sections, minimizing the tail of the zero-loss peak is as important as achieving a small half-width at half-maximum, in particular for detecting optical phonons in crystalline solids around 50 meV [6,8]. The scattering geometry in the electron microscope suggests that bond stretching in the specimen plane or longitudinal optical phonons will dominate the scattering [8]. Radiation damage is an issue for sensitive samples, in particular organic specimens, and aloof beam imaging conditions have been considered in this context [9,10].

There has been considerable discussion as to whether phonon scattering can give high-resolution images [7,11–13], in particular since energy losses are small (of the order of meV for single-phonon excitation). Atomic resolution is indeed possible, as discussed in Ref. [13], and this should not come as a surprise since atomic-resolution high-angle annular dark-field (HAADF) imaging, also known as Z-contrast imaging, is based on detecting electrons which have been scattered to large angles after (multiple) phonon excitation. In HAADF imaging we are effectively integrating the signal from those electrons in the phonon sector of the low-loss spectrum which have been scattered into a range of angles defined by the HAADF detector. The possibility of obtaining time-resolved information from meV EELS data has also been discussed [14].

Electrons scattered by the excitation of phonons to even larger angles than in HAADF imaging have been utilized in what has been dubbed electron Rutherford backscattering (ERBS) [15]. In ERBS an energy-loss spectrum is obtained for a range of scattering angles near the backward direction, corresponding to a range of large momentum transfers. Multiple phonon excitations are involved in inelastic scattering to a detector spanning a solid angle in the backwards direction and energy losses in the eV range are typical for incident energies of tens of keV. Peaks in the spectra correspond to the different atomic masses in the specimen [15]. The ERBS spectra are usually explained in a classical model, considering the recoil of electrons after quasielastic scattering and with the inclusion of Doppler broadening (due to the motion of the atoms). The theme of weighing individual atoms by high-angle scattering of electrons has recently been further explored, also in terms of classical models [16,17]. Site-specific recoil diffraction of backscattered electrons in crystals and the effects of channeling on spectra have also been investigated [18,19].

As early as 1955, Glauber proposed a time-dependent correlation function to model inelastic scattering via excitations of a crystal lattice [20]. General expressions for the various orders of thermal diffuse scattering were given by Borie [21]. Whelan [22] and Hall and Hirsch [23] examined phonon excitation by high-energy electrons in an Einstein model. This work was later expanded upon by Earney [24]. In this paper we discuss a fundamental approach to modeling the phonon-loss sector of the energy-loss spectrum based on considering the transition potentials between initial and final

*lja@unimelb.edu.au

states of the phonon subsystem, i.e., the states describing the nuclear motion. A correlated model is used for calculating the vibrational modes of the system and these results are contrasted with the simpler Einstein model in which atoms in the specimen are assumed to vibrate independently in potential wells provided by all the other charged particles in the specimen. These models incorporate the effects of multiphonon scattering (the creation or destruction of multiple phonons in a single scattering event); multiple phonon scattering (where phonons are created or destroyed in a series of independent scattering events) is not considered. Low-loss spectra for silicon are calculated for both plane-wave illumination of the specimen and for the case of an atomic-scale focused coherent probe in STEM, exploring the variation of the spectrum as a function of the position of the STEM probe and how it is affected by the size of the spectrometer aperture. We discuss how the quantum mechanical correlated and Einstein models for phonon excitation relate to classical models.

II. INELASTIC SCATTERING CROSS SECTION

A general expression for the cross section for inelastic scattering of an electron in a crystal is given by [25–27]

$$\sigma = \frac{2\pi m}{h^2 k_0} \iint \psi_0^*(\mathbf{r}) W(\mathbf{r},\mathbf{r}') \psi_0(\mathbf{r}')\, d\mathbf{r} d\mathbf{r}', \tag{1}$$

where h is the Planck constant and m, k_0, and $\psi_0(\mathbf{r})$ are the mass, wave number, and wave function of the incident electron respectively. The nonlocal potential $W(\mathbf{r},\mathbf{r}')$ for inelastic scattering is given by

$$W(\mathbf{r},\mathbf{r}') = \frac{2\pi m}{h^2} \sum_{n\neq 0} k_n H_{n0}^*(\mathbf{r}) H_{n0}(\mathbf{r}') \times \int_{k'} \int_D e^{2\pi i \mathbf{k}'\cdot(\mathbf{r}-\mathbf{r}')} \delta(k_n - k')\, d\Omega_{k'} dk'. \tag{2}$$

Here k_n is the wave number of the incident electron after an inelastic scattering event which leaves the target, initially in a state labeled 0, in a state labeled by n. The quantities $H_{n0}(\mathbf{r})$ are the transition potentials, defined as

$$H_{n0}(\mathbf{r}) = \int a_n^*(\boldsymbol{\tau}) H'(\mathbf{r},\boldsymbol{\tau}) a_0(\boldsymbol{\tau})\, d\boldsymbol{\tau}, \tag{3}$$

where $a_n(\boldsymbol{\tau})$ is the wave function describing the nth state of the target, $\boldsymbol{\tau}$ representing the nuclear coordinates. (We restrict our attention to modeling the states of the phonon subsystem, since we are interested specifically in the phonon-loss sector of the energy-loss spectrum and assume that the electronic degrees of freedom have been integrated out [28].) In Eq. (3) the quantity $H'(\mathbf{r},\boldsymbol{\tau})$ is the interaction Hamiltonian between the incident electron and the nuclear subsystem. The second line in Eq. (2) is an integration over the range of wave vectors $\mathbf{k}'$, for the scattered fast electron, into a detector D with solid angle $d\Omega_{k'}$, while maintaining conservation of energy. The summation in Eq. (2) over all final states corresponding to a particular energy loss then allows the calculation of a point in an energy-loss spectrum via Eq. (1).

By inserting Eq. (2) into Eq. (1) we obtain

$$\begin{aligned}
\sigma &= \frac{2\pi m}{h^2 k_0} \iint \psi_0^*(\mathbf{r}) \left[\frac{2\pi m}{h^2} \sum_{n\neq 0} H_{n0}^*(\mathbf{r}) H_{n0}(\mathbf{r}') k_n \int_{k'} \int_D e^{2\pi i \mathbf{k}'\cdot(\mathbf{r}-\mathbf{r}')} \delta(k_n - k')\, d\Omega_{k'} dk' \right] \psi_0(\mathbf{r}')\, d\mathbf{r} d\mathbf{r}' \\
&= \frac{4\pi^2 m^2}{h^4} \sum_{n\neq 0} \frac{k_n}{k_0} \int_{k'} \int_D \left[\int \psi_0^*(\mathbf{r}) H_{n0}^*(\mathbf{r}) e^{2\pi i \mathbf{k}'\cdot\mathbf{r}}\, d\mathbf{r} \right] \left[\int \psi_0(\mathbf{r}') H_{n0}(\mathbf{r}') e^{-2\pi i \mathbf{k}'\cdot\mathbf{r}'}\, d\mathbf{r}' \right] \delta(k_n - k')\, d\Omega_{k'} dk' \\
&= \frac{4\pi^2 m^2}{h^4} \sum_{n\neq 0} \frac{k_n}{k_0} \int_{k'} \int_D \left| \int \psi_0(\mathbf{r}') H_{n0}(\mathbf{r}') e^{-2\pi i \mathbf{k}'\cdot\mathbf{r}'}\, d\mathbf{r}' \right|^2 \delta(k_n - k')\, d\Omega_{k'} dk' \\
&= \frac{4\pi^2 m^2}{h^4} \sum_{n\neq 0} \frac{k_n}{k_0} \int_{k'} \int_D \left| \int \psi_0(\mathbf{k}' - \mathbf{q}') H_{n0}(\mathbf{q}')\, d\mathbf{q}' \right|^2 \delta(k_n - k')\, d\Omega_{k'} dk'.
\end{aligned} \tag{4}$$

We have expressed the inelastic scattering cross section in terms of the convolution between the probe wave function and the transition potentials in reciprocal space. This formulation is more amenable to analysis in later sections. For the case of plane wave incidence we have $\psi_0(\mathbf{r}) = \exp(2\pi i \mathbf{k}_0 \cdot \mathbf{r})$, where $\mathbf{k}_0$ is the incident wave vector, or equivalently $\psi_0(\mathbf{k}') = \delta(\mathbf{k}' - \mathbf{k}_0)$. The inelastic scattering cross section can then be expressed in terms of the quantities $H_{n0}(\mathbf{q})$ only, for which the modulus squared gives the probability for a transition in the specimen to state n initiated by a plane wave inelastically scattered into a point detector defined by the momentum transfer $h\mathbf{q} = h\mathbf{k}' - h\mathbf{k}_0$ as follows:

$$\sigma = \frac{4\pi^2 m^2}{h^4} \sum_{n\neq 0} \frac{k_n}{k_0} \int_{k'} \int_D |H_{n0}(\mathbf{q})|^2 \delta(k_n - k')\, d\Omega_{k'} dk'. \tag{5}$$

To evaluate the transition potentials $H_{n0}(\mathbf{q})$ we need to model the initial and final states of the target in Eq. (3), denoted by $a_0(\boldsymbol{\tau})$ and $a_n(\boldsymbol{\tau})$ respectively. The interatomic forces in a solid lead to correlated atomic motion in a range of normal vibrational modes. Within the harmonic approximation, these vibrational modes are decoupled and each obeys the wave equation for a quantum harmonic oscillator. This is the traditional approach of Born–von Kármán lattice dynamics [29]. In the simpler Einstein model each nucleus vibrates independently within an effective confining potential due to all the other charged particles in the specimen. In other words, each nucleus is assumed to be confined in a three-dimensional potential (assumed harmonic), whose frequencies are chosen so that the root-mean-squared (rms) displacement of every atom from the equilibrium position

(the electrons are assumed to move with the nucleus) matches either experimental data or theoretical prediction. The Einstein model has been used with great success in simulations of transmission electron microscope images, in those imaging modes where one is not interested in the details of the phonon sector of the energy-loss spectrum but where integration over some elements of the spectrum is pertinent, for example, Refs. [30–32]. In general we do not expect the Einstein model to yield an accurate prediction of the phonon-loss spectrum. We will discuss later situations where the Einstein model might be expected to yield a reasonable approximation for the spectrum.

Lastly, in this section, we note that we are considering incident electrons with incident energies of the order of tens or hundreds of keV, so that relativistic effects need to be taken into account. This is done as discussed in Ref. [33].

III. TRANSITION POTENTIALS

Replacing the generic label n in Eq. (3) explicitly with a vector $\mathbf{n}$ containing the quantum numbers n_j each associated with a normal mode of vibration labeled by j, the transition potential for exciting the lattice to the state $\mathbf{n}$ is given by [34]

$$H_{\mathbf{n}0}(\mathbf{q}) = \frac{h^2}{2\pi m}\sum_{\kappa} e^{-2\pi i \mathbf{q}\cdot\mathbf{R}_\kappa} f_e^\kappa(\mathbf{q}) \times \prod_j \frac{\left[-i\sqrt{2\frac{M_j}{m_\kappa}}\mathbf{q}\cdot\boldsymbol{\varepsilon}_j^\kappa\right]^{n_j}}{\sqrt{n_j!}} e^{-\frac{M_j}{m_\kappa}(\mathbf{q}\cdot\boldsymbol{\varepsilon}_j^\kappa)^2} \quad (6)$$

and the transition probability is therefore given by

$$|H_{\mathbf{n}0}(\mathbf{q})|^2 = \frac{h^4}{4\pi^2 m^2}\sum_{\kappa} f_e^\kappa(\mathbf{q})^2 \prod_j \frac{\left[2\frac{M_j}{m_\kappa}\left(\mathbf{q}\cdot\boldsymbol{\varepsilon}_j^\kappa\right)^2\right]^{n_j}}{n_j!} \times e^{-2\frac{M_j}{m_\kappa}(\mathbf{q}\cdot\boldsymbol{\varepsilon}_j^\kappa)^2} + \text{cross terms}, \quad (7)$$

where the cross terms (i.e., those terms arising from the interference between scatter off distinct atoms) are not written out explicitly.

In Eqs. (6) and (7) the equilibrium position of atom κ (with mass m_κ) is denoted by $\mathbf{R}_\kappa$. The electron scattering factors $f_e^\kappa(\mathbf{q})$ for atom type κ are those for isolated atoms and we use the parametrization of Waasmeier and Kirfel [35]. Since we are assuming isolated atoms, any long-range dipole interactions which result from charge redistribution due to bonding [12] are neglected. Here we are considering direct interaction with the nuclear subsystem rather than indirectly via long-range interactions with the electronic subsystem, as is the case in aloof beam imaging [1,10]. The Debye-Waller factors M_j are given by [34]

$$M_j = \pi^2 \frac{\hbar}{\omega_j}, \quad (8)$$

where $\hbar$ is the reduced Planck constant and ω_j is the frequency of the normal vibrational mode j. In what follows, the reader should bear in mind that all frequencies will be implicit in the Debye-Waller factors. These Debye-Waller factors can be modified to include the effects of nonzero temperature according to Bose-Einstein statistics by including the factor $\coth(\hbar\omega_j/2k_\mathrm{B}T)$ [34]. The polarization vectors $\boldsymbol{\varepsilon}_j^\kappa$ for the atom κ in the mode j are defined in terms of eigenvectors obtained by solving the lattice dynamical eigenvalue problem which can be stated in the form [29]

$$\sum_{\kappa'=1}^{n_\mathrm{u}} \mathbf{D}^{\kappa\kappa'}\boldsymbol{\epsilon}^{\kappa'} = \omega^2\boldsymbol{\epsilon}^\kappa. \quad (9)$$

Here κ and κ' run over the atoms within the unit cell, n_u is the number of atoms in the unit cell, $\boldsymbol{\epsilon}^\kappa$ is an eigenvector for atom κ, and $\mathbf{D}^{\kappa\kappa'}$ is the dynamical matrix which describes the forces between atoms κ and κ'. The dynamical matrix depends on the phonon wave vector $\mathbf{k}$ and the eigenvalue problem is solved separately for each wave vector in the first Brillouin zone. The number of eigenvalue-eigenvector pairs for each phonon wave vector is in general $3n_\mathrm{u}$ (corresponding to the three Cartesian directions in which each atom can move), except in the case of phonon wave vectors pointing in high symmetry directions for which degeneracies may occur [36]. Each of these $3n_\mathrm{u}$ pairs is referred to as a *branch*. For silicon, with two atoms in the (primitive) unit cell, there are six such branches. We use the notation $\boldsymbol{\epsilon}_j^\kappa$ to denote the polarization vector of the κth atom in the mode j. These modes j are enumerated by first running over all the phonon wave vectors $\mathbf{k}$ in the first Brillouin zone for which $-\mathbf{k}$ is also in the first Brillouin zone, considering all branches, and then including both classes of normal modes, defined by $m = 1,2$, in the following equation:

$$\boldsymbol{\varepsilon}_j^\kappa = \frac{\mathrm{i}^{m-1}}{\sqrt{2N}}\left\{\boldsymbol{\epsilon}^\kappa \exp\left[2\pi i\mathbf{k}\cdot\mathbf{R}_\kappa^\mathrm{u}\right] + (-1)^{m-1}\boldsymbol{\epsilon}^{\kappa *}\exp\left[-2\pi i\mathbf{k}\cdot\mathbf{R}_\kappa^\mathrm{u}\right]\right\}. \quad (10)$$

Here N is the number of unit cells. We note that the two classes of modes defined by $m = 1,2$ arise because the eigenvectors are in general complex and the real and imaginary parts constitute independent modes of vibration corresponding to physical displacements of the nuclei. The index κ in Eq. (10) runs over all atoms in the supercell and $\mathbf{R}_\kappa^\mathrm{u}$ refers to the origin of the unit cell in which the atom κ sits. For the wave vectors which are on the Brillouin zone boundary (which correspond intrinsically to standing wave modes) we run over all branches as before but take only one of the classes of normal modes defined by $m = 1,2$. An alternative approach is to retain all the vectors in the first Brillouin zone at the outset and take one class of solutions [36]. In either approach, the total number of modes will be $3n_\mathrm{u}N$.

The force constant model used to define the dynamical matrix can be fitted against experimental data, such as neutron diffraction data [37], or it can come from density functional theory [38]. We note that even though Born–von Kármán lattice dynamics is a classical approach to lattice dynamics, the procedure for determining the normal modes of vibration and their frequencies is equivalent to working from a fundamentally quantum mechanical approach in which the potential for the target is written down and the Hamiltonian diagonalized [29]. Thereafter the Schrödinger equation can be separated to describe decoupled quantum harmonic oscillators.

In Fig. 1 we show two of the many possible transition probabilities for the excitation of bulk phonons in a silicon crystal, assumed infinite in all directions (so that we are

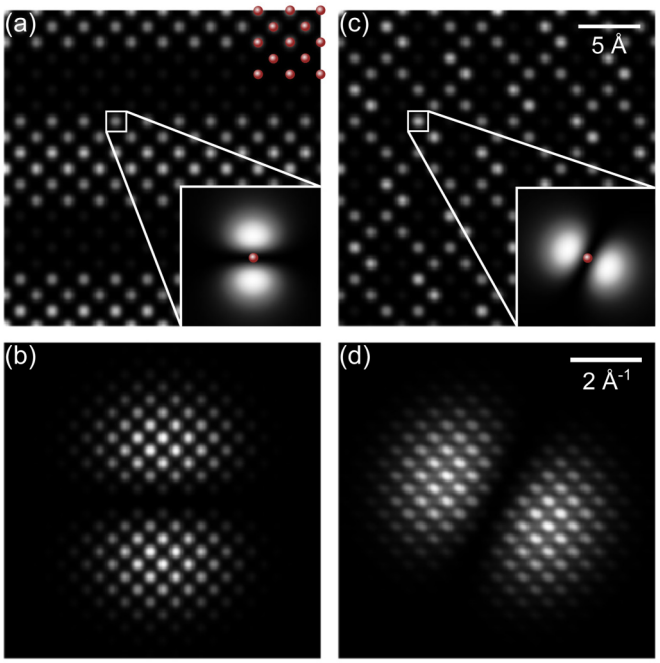

FIG. 1. (a) Transition probability in real space $|H_{n0}(\mathbf{r})|^2$ projected along [001] for a longitudinal optical phonon with wave vector $\mathbf{k} = (-0.2,0,0)$, for $m = 1$ and corresponding to an energy loss of 63.6 meV. The image has been blurred for the purposes of visualisation using a Gaussian kernel of FWHM 0.33 Å. The inset is a blowup of the area indicated (encompassing one atom, position indicated), without blurring. (b) Transition probability in reciprocal space $|H_{n0}(\mathbf{q})|^2$ for the phonon mode in panel (a), blurred with a FWHM of 0.11 Å^{-1}. (c) Transition probability in real space for a longitudinal acoustic phonon with wave vector $\mathbf{k} = (-0.2,-0.4,0)$, for $m = 1$ and corresponding to an energy loss of 25.2 meV, blurred as in panel (a). The inset is a blowup of the area indicated (encompassing one atom, position indicated), without blurring. (d) Transition probability in reciprocal space for the phonon mode in panel (d), blurred as in panel (b). The projected structure of the conventional cubic unit cell is overlaid on panel (a). The scale bar on panel (c) also applies to panel (a) and that on panel (d) also to panel (b).

not considering surface phonons). In practice we work on a supercell, which is a $5 \times 5 \times 5$ tiling of the conventional cubic unit cell, which corresponds to $N = 500$ primitive unit cells, and hence there are 3000 modes j. Figure 1(a) shows the transition probability in real space $|H_{n0}(\mathbf{r})|^2$ projected along [001] for a longitudinal optical phonon with wave vector $\mathbf{k} = (-0.2,0,0)$, for $m = 1$ in Eq. (10), and which has an energy loss of 63.6 meV. Figure 1(b) shows the transition probability in reciprocal space $|H_{n0}(\mathbf{q})|^2$ for the phonon mode in Fig. 1(a). Figures 1(c) and 1(d) show analogous results to those in Figs. 1(a) and 1(b) but now for an acoustic phonon with wave vector $\mathbf{k} = (-0.2,-0.4,0)$ and $m = 1$ with a corresponding energy loss of 25.2 meV. Note that the transition potentials go to zero on the atomic site and peak to either side. This is characteristic of potentials for single-phonon excitation [12]. These structural features are pertinent when imaging with an atomic-sized probe, as we will discuss later.

We now consider the form of the transition potentials in an Einstein model. For excitation of atom κ into the state $\mathbf{n}^\kappa = (n_1^\kappa, n_2^\kappa, n_3^\kappa)$ (where 1,2,3 refer to the Cartesian directions) we have [34]

$$H_{\mathbf{n}^\kappa 0}(\mathbf{q}) = \frac{h^2}{2\pi m} e^{-2\pi i \mathbf{q}\cdot\mathbf{R}_\kappa} f_e^\kappa(\mathbf{q}) \times \prod_i \frac{\left[-i\sqrt{2\frac{M_i^\kappa}{m_\kappa}} q_i^2\right]^{n_i^\kappa}}{\sqrt{n_i^\kappa!}} e^{-\frac{M_i^\kappa}{m_\kappa} q_i^2} \tag{11}$$

and the transition probability is given by

$$|H_{\mathbf{n}^\kappa 0}(\mathbf{q})|^2 = \left(\frac{h^2}{2\pi m}\right)^2 f_e^\kappa(\mathbf{q})^2 \prod_i \frac{\left[2\frac{M_i^\kappa}{m_\kappa} q_i^2\right]^{n_i^\kappa}}{n_i^\kappa!} e^{-2\frac{M_i^\kappa}{m_\kappa} q_i^2}. \tag{12}$$

Here, the index i runs over the Cartesian directions and M_i^κ are the Debye-Waller factors for the κth atom. As alluded to in the previous section, these Debye-Waller factors are chosen such that the rms displacements agree with the prediction of the correlated model. This can be expressed as the condition

$$M_i^\kappa = \sum_j \left(\varepsilon_{ji}^\kappa\right)^2 M_j, \tag{13}$$

where ε_{ji}^κ is the ith Cartesian component of the polarization vector $\boldsymbol{\varepsilon}_j^\kappa$.

Next we consider the case of single-phonon excitation for both the correlated model and the Einstein model. When the incident electron scatters via small angles, i.e., $\mathbf{q}$ is small and $\mathbf{q} \approx \mathbf{q}_\perp$, it is a reasonable approximation to include only single-phonon excitation. In this case, the transition probability for singly exciting the jth mode within the correlated model is given by

$$|H_{(1j)0}(\mathbf{q})|^2 = \left(\frac{h^2}{2\pi m}\right)^2 \sum_\kappa f_e^\kappa(\mathbf{q})^2 \left[2\frac{M_j}{m_\kappa}\left(\mathbf{q}\cdot\boldsymbol{\varepsilon}_j^\kappa\right)^2\right] + \text{cross terms}, \tag{14}$$

where the label $1j$ indicates that the final state includes a single excitation of only the jth mode. In the Einstein model, the probability of singly exciting the ith Cartesian mode of the κth atom is given by

$$|H_{(1\kappa i)0}(\mathbf{q})|^2 = \left(\frac{h^2}{2\pi m}\right)^2 f_e^\kappa(\mathbf{q})^2 \left[2\frac{M_i^\kappa}{m_\kappa} q_i^2\right], \tag{15}$$

where the label $1\kappa i$ indicates that the final state includes a single excitation of only the ith Cartesian mode of the κth atom. It should be noted that since we are considering small scattering vectors $\mathbf{q}$, we have made the approximation that $\exp[-M_j(\mathbf{q}\cdot\boldsymbol{\varepsilon}_j^\kappa)^2/m_\kappa] \approx 1$.

We will now show that, for single-phonon excitation, integrating the spectra over energy yields the same result in the correlated and Einstein models. The sum over all single-excitation transition probabilities in the Einstein model is found by summing over the result in Eq. (15) for each atom

κ and each Cartesian degree of freedom i:

$$\left(\frac{h^2}{2\pi m}\right)^2 \sum_\kappa f_e^\kappa(\mathbf{q})^2 \sum_i \left[2\frac{M_i^\kappa}{m_\kappa} q_i^2\right]$$
$$= \left(\frac{h^2}{2\pi m}\right)^2 \sum_\kappa f_e^\kappa(\mathbf{q})^2 \sum_i \left[\frac{2}{m_\kappa}\left(\sum_j \varepsilon_{ji}^{\kappa\,2} M_j\right) q_i^2\right]$$
$$= \left(\frac{h^2}{2\pi m}\right)^2 \sum_\kappa f_e^\kappa(\mathbf{q})^2 \sum_j \left[2\frac{M_j}{m_\kappa}\sum_i \left(q_i \varepsilon_{ji}^\kappa\right)^2\right]$$
$$= \left(\frac{h^2}{2\pi m}\right)^2 \sum_\kappa f_e^\kappa(\mathbf{q})^2 \sum_j \left[2\frac{M_j}{m_\kappa}\left(\mathbf{q}\cdot\boldsymbol{\varepsilon}_j^\kappa\right)^2\right], \quad (16)$$

where Eq. (13) is used in going from the first to the second line. The final line above is a sum over all modes j of the transition probabilities in the correlated model as given in Eq. (14), provided that we work within the incoherent approximation, wherein the cross terms in Eq. (14) are neglected. This is a reasonable approximation in practice when collecting the inelastically scattered electrons into the range of angles permitted by the detector, as we have verified numerically, and which is also consistent with the results in Ref. [39]. Thus in a single-phonon model, although the details of the spectra may be quite different, the integrated spectra of the two models are identical.

The proof can be extended to all orders of scattering: It turns out to hold for every individual order of scattering; i.e., the integrated spectrum for two-phonon processes is identical in the two models, and so on for three-phonon, four-phonon processes, etc. Once again we will work within the incoherent approximation; i.e., we ignore the cross terms in Eq. (7). For clarity we now restrict our attention to a single atom at a time and thus drop the κ index, and additionally write the transition probability within the Einstein model as

$$|H_{\mathbf{n}0}|^2 = \left(\frac{h^2}{2\pi m}\right)^2 f_e(\mathbf{q})^2 G_{\mathbf{n}0} \quad (17)$$

so that we have

$$G_{\mathbf{n}0} = \prod_i \frac{\left[2\frac{M_i}{m} q_i^2\right]^{n_i}}{n_i!} e^{-2\frac{M_i}{m} q_i^2}. \quad (18)$$

The total probability P_n of n-phonon scattering processes is proportional to

$$\sum_{\sum_i n_i = n} G_{\mathbf{n}0} = \sum_{\sum_i n_i = n} \prod_i \frac{\left[2\frac{M_i}{m} q_i^2\right]^{n_i}}{n_i!} e^{-2\frac{M_i}{m} q_i^2}$$
$$= \frac{\left[\sum_i 2\frac{M_i}{m} q_i^2\right]^n}{n!} e^{-\sum_i 2\frac{M_i}{m} q_i^2}, \quad (19)$$

where we have used the multinomial theorem

$$\frac{\left(\sum_i x_i\right)^n}{n!} = \sum_{\sum_i n_i = n} \prod_i \frac{x_i^{n_i}}{n_i!}. \quad (20)$$

Substituting for the Debye-Waller factors M_i using Eq. (13) we have

$$P_n \propto \frac{\left[\sum_i \frac{2}{m}\left(\sum_j \varepsilon_{ji}^2 M_j\right) q_i^2\right]^n}{n!} e^{-\sum_i \frac{2}{m}\left(\sum_j \varepsilon_{ji}^2 M_j\right) q_i^2}$$
$$= \frac{\left[\sum_j 2\frac{M_j}{m}(\mathbf{q}\cdot\boldsymbol{\varepsilon}_j)^2\right]^n}{n!} e^{-\sum_j 2\frac{M_j}{m}(\mathbf{q}\cdot\boldsymbol{\varepsilon}_j)^2}$$
$$= \sum_{\sum_j n_j = n} \prod_j \frac{\left[2\frac{M_j}{m}(\mathbf{q}\cdot\boldsymbol{\varepsilon}_j)^2\right]^{n_j}}{n_j!} e^{-2\frac{M_j}{m}(\mathbf{q}\cdot\boldsymbol{\varepsilon}_j)^2}, \quad (21)$$

where in going from the second line to the third line we have once again used the multinomial theorem. The final line is proportional to the total probability within the correlated model of all n-phonon scattering processes. Therefore, assuming the incoherent approximation, the integrated spectrum in the correlated and Einstein models will be the same in general.

IV. SPECTRA FOR SILICON

A spectrum calculated in the correlated model for silicon illuminated by a plane wave down [001] at 300 keV and considering only single-phonon excitation, which predominates in the forward direction, is shown in Fig. 2(a). The correlated modes which contribute in Fig. 2(a) were calculated using Eq. (9), with the force constant parameters for the dynamical matrix taken from Ref. [37]. We note that this spectrum is not simply the phonon density of states for silicon (see Ref. [40]) divided by frequency, due to the dependence of the transition potential in Eq. (6) on the wave vector transfer $\mathbf{q}$ and the polarization vectors $\boldsymbol{\varepsilon}_j^\kappa$. The corresponding spectrum in the Einstein model, also assuming single-phonon excitation, is shown for comparison. The spectra in Fig. 2(a) have a Gaussian blur with standard deviation of 1 meV applied to simulate experimental energy broadening. While the integrated spectra are the same, as expected from the reasoning at the end of the last section, the details of the spectra are substantially different. A simulation in the correlated model for scattering in the strictly backward direction is computationally challenging due to the very large number of multiphonon final states associated with the different modes. Therefore we have confined ourselves to a quantum mechanical calculation in the Einstein model, shown in Fig. 2(b), and we have reason to believe that the correlated model would give similar results, as we will discuss in the next section. We have also shown in Fig. 2(b) the spectrum predicted by a classical model of elastic scattering from a quasifree atom, including Doppler broadening [15]. We note that the two spectra in Fig. 2(b) agree closely in both the location of the peak energy loss and the width of the peak.

Next we consider the variation in the spectrum when a small atomic-sized coherent probe, as in atomic-resolution STEM, is scanned across the specimen and the results are recorded in a spectrometer with a small aperture in the forward direction. Assuming an incident energy of 300 keV, a probe forming aperture of 15 mrad, and a detector semiangle of 5 mrad, we see in Fig. 3 that as the probe scans across the positions indicated on the inset (showing the projected structure of

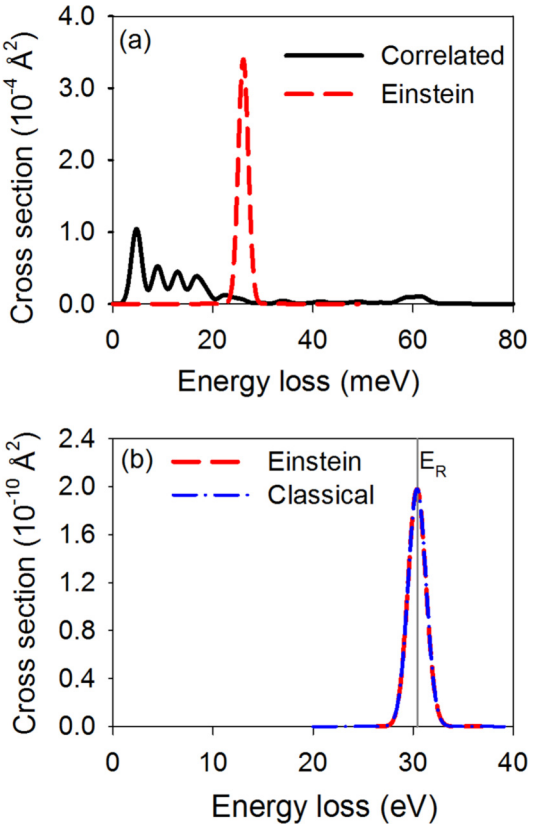

FIG. 2. Phonon-loss spectra for 300-keV plane-wave electrons incident on silicon down [001], calculated at room temperature. (a) Spectrum obtained for single-phonon excitation in both the correlated and Einstein models, which is dominated by scattering in the forward direction. (b) Spectrum in the strictly backwards direction for the Einstein model, taking into account multiphonon excitation, and a classical model incorporating Doppler broadening. The peak value occurs at the classical recoil energy E_R, indicated by the solid line. The Einstein and classical model results in panel (b) have been normalized to each other and are almost indistinguishable.

silicon along [001]) that not only does the overall scattering vary as a function of probe position but the shape of the spectrum also changes substantially. This can be understood by examining the third line in Eq. (4), where we see the overlap between the probe and the transition potential in the factor $\psi_0(\mathbf{r}')H_{n0}(\mathbf{r}')$; clearly an atomic-sized probe will interact differently with each transition potential at different probe positions. This is evident from the insets in Figs. 1(a) and 1(c). It is interesting to note that when the probe is on a column of silicon atoms (position 1) the integrated spectrum is considerably less than when it is just off the column (position 2). The reason for this is that, despite there being more overall inelastic scattering when the probe is on the column, there is a redistribution of scattering intensity out to larger angles when the probe is on the column, in such a way that there is less intensity inside a small aperture than when the probe is off the column. The size of the spectrometer aperture will thus be an important consideration in the development of techniques for atomic-resolution vibrational spectroscopy.

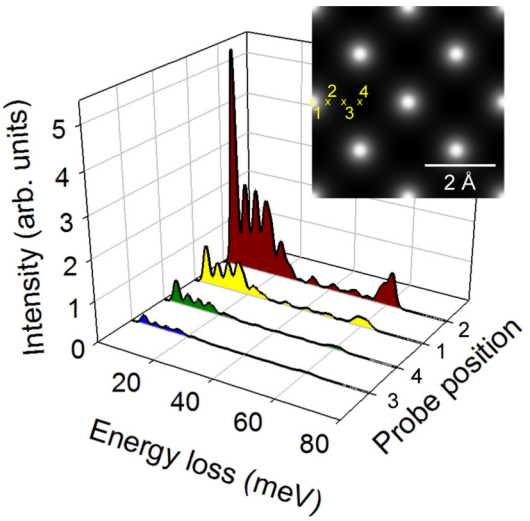

FIG. 3. Spectra (in arbitrary units) as a function of energy loss in meV, for the four equally spaced probe positions as indicated in the schematic of the cubic unit cell (inset, viewed along [001]) and presented in the order indicated for purposes of visualization. All spectra are on the same absolute scale. Besides variations in magnitude, variations in shape are evident.

V. RELATIONSHIP BETWEEN MODELS

We have already seen in previous sections some ways in which the correlated model and the Einstein model are related. Let us recap here. In the forward direction, unlike the correlated model, the Einstein model will, in general, not predict the details of the phonon-loss spectrum correctly. However, as we have shown both analytically in the incoherent approximation and by numerical example, the Einstein model does give the integrated intensity, i.e., the total scattering due to phonon excitation, correctly. An effective Einstein model can be constructed from the detailed phonon model by matching the mean-squared displacements of all atoms, as encapsulated in Eq. (13). We have also seen that for the spectrum shown in Fig. 2(b), the Einstein model spectrum has its maximum at the classical recoil energy. Let us now explore what happens to the correlated model spectrum for scattering to large angles.

Once again making the incoherent approximation in Eq. (7), i.e., ignoring the cross terms, we have for atom κ that the probability of the transition from the ground state to the final state $\mathbf{n} = (n_1, \ldots, n_j, \ldots)$ is given by

$$\left|H^{\kappa}_{\mathbf{n}0}(\mathbf{q})\right|^2 = \frac{h^4}{4\pi^2 m^2} f_e^{\kappa}(\mathbf{q})^2 \times \prod_j \frac{\left[2\frac{M_j}{m_\kappa}\left(\mathbf{q}\cdot\boldsymbol{\varepsilon}^{\kappa}_j\right)^2\right]^{n_j}}{n_j!} e^{-2\frac{M_j}{m_\kappa}(\mathbf{q}\cdot\boldsymbol{\varepsilon}^{\kappa}_j)^2}. \quad (22)$$

This expression is composed of factors of the form $\frac{x^n}{n!}\exp(-x)$, which are maximized when $x \approx n$. This approximation becomes better as n becomes larger. In other words, Eq. (22) is maximized when

$$n_j \approx 2\frac{M_j}{m_\kappa}\left(\mathbf{q}\cdot\boldsymbol{\varepsilon}^{\kappa}_j\right)^2. \quad (23)$$

The approximation is better at larger scattering angles, where the total number n of phonons excited is large. When this is true it is either the case that the n_j in Eq. (23) are sufficiently large for the approximation to be a good one or that alternatively there are many modes j for which the right-hand side of Eq. (23) is sufficiently similar that those modes may be concatenated together and considered as one, leading to an effectively large n_j.

Assuming that Eq. (23) is reasonably well satisfied we have that the total energy loss (across all degrees of freedom) is given by

$$E_{\rm loss} = \sum_j n_j \hbar\omega_j \approx \sum_j 2\frac{M_j}{m_\kappa}\left(\mathbf{q}\cdot\boldsymbol{\varepsilon}_j^\kappa\right)^2\hbar\omega_j\ . \tag{24}$$

Using the fact that $M_j = \pi^2\hbar/\omega_j$ [see Eq. (8)] we can now write

$$E_{\rm loss} \approx \frac{h^2}{2m_\kappa}\sum_j\left(\mathbf{q}\cdot\boldsymbol{\varepsilon}_j^\kappa\right)^2 \approx \frac{h^2}{2m_\kappa}q^2 = E_{\rm R}, \tag{25}$$

where $E_{\rm R} = h^2q^2/2m_\kappa$ is the classical recoil energy. The second approximation, that $\sum_j(\mathbf{q}\cdot\boldsymbol{\varepsilon}_j^\kappa)^2 \approx q^2$, is accurate for a crystal lattice with sufficient symmetry and is exact for a Bravais lattice with centrosymmetry such as silicon [41]. We have also verified numerically that this is indeed the case. This result indicates that when the approximation in Eq. (23) is reasonable, then the spectrum will have its peak energy loss at the classical recoil energy. As pointed out earlier, it is computationally challenging to check this result for the present study of silicon due to the large number of final states involved. However, as we have seen in Fig. 2(b), the Einstein model spectrum also agrees with the classical prediction, taking into account Doppler broadening (i.e., the atomic motion), as described in Ref. [15]. This is consistent with analogous studies in neutron scattering that for a phonon density of states sufficiently characterized by a single lattice frequency the probability distribution for large n-phonon processes is distributed as a Gaussian about the mean recoil energy [41]. It is reasonable to speculate that the correlated model would coincide with both of these models in the backward direction.

Let us consider the relationship between the Einstein and classical models in more detail. We begin by considering an atom sitting in an isotropic harmonic well defined by a trap frequency ω corresponding to a silicon atom in crystalline silicon at room temperature. From Eq. (5) the differential cross section for scattering into the solid angle Ω via excitation of the target to the state $\mathbf{n}$ is given by

$$\frac{d\sigma_{\mathbf{n}}}{d\Omega} = \frac{4\pi^2m_e^2}{h^2}|H_{\mathbf{n}0}(\mathbf{q})|^2\ , \tag{26}$$

where $H_{\mathbf{n}0}(\mathbf{q})$ is the transition potential, given in the Einstein model by Eq. (11). Many of the final states described by the vectors $\mathbf{n}$ correspond to the same energy loss, and so we sum over all such states to obtain the differential cross section for a scalar $n = \sum_i n_i$. The energy loss associated with the quantum number n is $E_{\rm loss} = n\hbar\omega$. There is furthermore a dependence on the azimuthal angle ϕ due to the choice of coordinate system and we thus define a differential cross section with respect to θ by averaging over ϕ:

$$\frac{d\sigma_n}{d\theta} \equiv \frac{1}{2\pi}\int d\phi\,\frac{d\sigma_n}{d\Omega}. \tag{27}$$

It can be shown after some algebra that this reduces to

$$\frac{d\sigma_n}{d\theta} = f_e^2(\mathbf{q})\frac{k_n}{k_0}\frac{(2Mq^2)^n}{n!}e^{-2Mq^2}, \tag{28}$$

where q^2 is the square of the scattering vector, given by

$$q^2 = k_0^2 + k_n^2 - 2k_0k_n\cos\theta. \tag{29}$$

Assuming a constant scattering factor (a reasonable approximation for this purpose) and maximizing Eq. (28) with respect to θ, we find, to first order in the energy loss, the relationship

$$\cos\theta \approx 1 - \frac{m_\kappa}{m}\frac{1}{\gamma+1}\frac{E_{\rm loss}}{E}, \tag{30}$$

where γ is the relativistic Lorentz factor. This is the same result that is found from a relativistic classical analysis, assuming that the energy loss is the recoil energy of the target [15,16]. The small energy loss approximation is reasonable since the energy losses are of the order of eV or tens of eV, as compared with the typical incident energies of tens or hundreds of keV. Equation (28) can be recast in terms of energy loss and the scattering angle θ by substituting Eq. (29) for q^2 and $E_{\rm loss}/\hbar\omega$ for n.

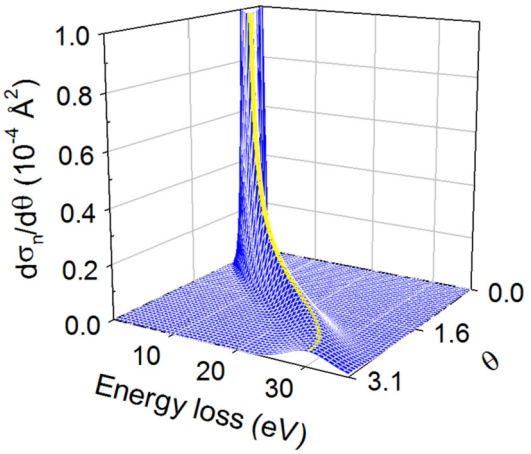

FIG. 4. Differential cross section as in Eq. (28) for a plane wave of incident energy 300 keV as a function of energy loss and scattering angle, calculated for a silicon atom in an isotropic harmonic oscillator potential with trap frequency $\omega = 4.6\times10^{14}$ s^{-1}. The overlaid (yellow) line is the classical relationship in Eq. (30).

Figure 4 shows what might be termed the *quantum kinematical surface*, which is the differential cross section in Eq. (28) as a function of energy loss and scattering angle, calculated for a plane wave of incident energy 300 keV and for a silicon atom in an isotropic harmonic oscillator potential with trap frequency $\omega = 4.6\times10^{14}$ s^{-1} (corresponding to a silicon atom at room temperature in crystalline silicon). The overlaid (yellow) line is the classical relationship in Eq. (30). The so-called ridge of the quantum kinematical surface tracks the classical prediction. This is a nice illustration of how quantum mechanics goes over to classical mechanics. Furthermore, we note that the width of the ridge, representing the extent to

which quantum mechanics is important, becomes smaller as the trap frequency is reduced.

VI. DISCUSSION AND CONCLUSION

We have discussed a fundamental theory to calculate the phonon-loss sector of the energy-loss spectrum for electrons scattering from crystalline solids based on transition potentials between initial and final states of the phonon sector of the target. Some properties of these transition potentials have been elucidated. We have used a correlated model to calculate the vibrational modes and spectra for silicon with both plane wave illumination and an atomic-scale focused coherent probe. For the latter case we have shown that the spectra depend on probe position. These spectra are also affected by the size of the aperture on the spectrometer. The correlated model has been contrasted with the Einstein model in which atoms in the specimen are assumed to vibrate independently. For small-angle scattering, the spectra predicted by the correlated and Einstein models are quite different. However, we have shown analytically that the integrated spectra are equal.

We have also discussed how both the correlated and Einstein models relate to a classical view of the energy-loss process. We have found that for scattering to large angles, the spectrum calculated within the correlated model will peak at roughly the energy loss predicted by the classical recoil energy, and that this will be the case at *all* angles in the Einstein model. The spectrum calculated in the Einstein model for large scattering angles (i.e., near the backward direction) has been shown to agree with a classical model of scattering from a quasifree atom including Doppler broadening, and there is reason to believe that this will also hold true for smaller scattering angles.

It remains to consider the effects of channeling and multiple inelastic (phonon) scattering (as opposed to multiphonon scattering considered here) on the measured spectra, the importance of which is well understood for core-loss spectroscopy; see, for example, Refs. [32,42].

ACKNOWLEDGMENT

This research was supported under the Australian Research Councils Discovery Projects funding scheme (Project No. DP110102228).

[1] O. L. Krivanek, T. C. Lovejoy, N. Dellby, T. Aoki, R. W. Carpenter, P. Rez, E. Soignard, J. Zhu, P. E. Batson, M. J. Lagos, R. F. Egerton, and P. A. Crozier, Nature (London) **514**, 209 (2014).
[2] H. Ibach, Phys. Rev. Lett. **24**, 1416 (1970).
[3] B. Schröder and J. Geiger, Phys. Rev. Lett. **28**, 301 (1972).
[4] O. Krivanek, N. Dellby, T. Lovejoy, N. Bacon, G. Corbin, P. Hrncirik, Z. S. Szilagyi, T. Aoki, R. W. Carpenter, P. A. Crozier *et al.*, Microsc. Microanal. **20**, 66 (2014).
[5] P. A. Crozier, J. Zhu, T. Aoki, P. Rez, W. J. Bowman, R. W. Carpenter, O. L. Krivanek, N. Dellby, T. C. Lovejoy, and R. F. Egerton, Microsc. Microanal. **20**, 72 (2014).
[6] R. F. Egerton, Microsc. Microanal. **20**, 658 (2014).
[7] R. Egoavil, N. Gauquelin, G. T. Martinez, S. Van Aert, G. Van Tendeloo, and J. Verbeeck, Ultramicroscopy **147**, 1 (2014).
[8] P. Rez, Microsc. Microanal. **20**, 671 (2014).
[9] A. Howie, Ultramicroscopy **11**, 141 (1983).
[10] R. F. Egerton, Ultramicroscopy **159**, 95 (2015).
[11] P. Rez, Ultramicroscopy **52**, 260 (1993).
[12] C. Dwyer, Phys. Rev. B **89**, 054103 (2014).
[13] N. R. Lugg, B. D. Forbes, S. D. Findlay, and L. J. Allen, Phys. Rev. B **91**, 144108 (2015).
[14] C. Li, G. Subramanian, and J. C. H. Spence, Microsc. Microanal. **20**, 837 (2014).
[15] M. R. Went and M. Vos, Nucl. Instrum. Methods Phys. Res., Sect. B **266**, 998 (2008).
[16] G. Argentero, C. Mangler, J. Kotakoski, F. Eder, and J. Meyer, Ultramicroscopy **151**, 23 (2015).
[17] T. C. Lovejoy, N. Dellby, T. Aoki, G. J. Corbin, P. Hrncirik, Z. S. Szilagyi, and O. L. Krivanek, Microsc. Microanal. **20**, 558 (2014).
[18] A. Winkelmann and M. Vos, Phys. Rev. Lett. **106**, 085503 (2011).
[19] A. Winkelmann and M. Vos, Ultramicroscopy **125**, 66 (2013).
[20] R. J. Glauber, Phys. Rev. **98**, 1692 (1955).
[21] B. Borie, Acta Crystallogr. **14**, 566 (1961).
[22] M. J. Whelan, J. Appl. Phys. **36**, 2103 (1965).
[23] C. R. Hall and P. B. Hirsch, Proc. R. Soc. London A **286**, 158 (1965).
[24] J. J. Earney, Philos. Mag. **23**, 577 (1971).
[25] L. J. Allen and T. W. Josefsson, Phys. Rev. B **52**, 3184 (1995).
[26] L. J. Allen, S. D. Findlay, M. P. Oxley, and C. J. Rossouw, Ultramicroscopy **96**, 47 (2003).
[27] S. D. Findlay, M. P. Oxley, and L. J. Allen, Microsc. Microanal. **14**, 48 (2008).
[28] B. D. Forbes, A. V. Martin, S. D. Findlay, A. J. DAlfonso, and L. J. Allen, Phys. Rev. B **82**, 104103 (2010).
[29] M. Born and K. Huang, *Dynamical Theory of Crystal Lattices* (Clarendon Press, Oxford, UK, 1954).
[30] J. M. LeBeau, S. D. Findlay, L. J. Allen, and S. Stemmer, Phys. Rev. Lett. **100**, 206101 (2008).
[31] J. M. LeBeau, S. D. Findlay, L. J. Allen, and S. Stemmer, Nano Lett. **10**, 4405 (2010).
[32] B. D. Forbes, A. J. D'Alfonso, R. E. A. Williams, R. Srinivasan, H. L. Fraser, D. W. McComb, B. Freitag, D. O. Klenov, and L. J. Allen, Phys. Rev. B **86**, 024108 (2012).
[33] C. J. Humphreys, Rep. Prog. Phys. **42**, 1825 (1979).
[34] A. V. Martin, S. D. Findlay, and L. J. Allen, Phys. Rev. B **80**, 024308 (2009).
[35] D. Waasmaier and A. Kirfel, Acta Crystallogr. Sect. A **51**, 416 (1995).
[36] B. T. M. Willis and A. W. Pryor, *Thermal Vibrations in Crystallography* (Cambridge University Press, Cambridge, UK, 1975), Vol. 1.
[37] W. Jian, Z. Kaiming, and X. Xide, Solid State Commun. **86**, 731 (1993).

[38] S. Baroni, S. De Gironcoli, A. Dal Corso, and P. Giannozzi, Rev. Mod. Phys. **73**, 515 (2001).
[39] D. A. Muller, B. Edwards, E. J. Kirkland, and J. Silcox, Ultramicroscopy **86**, 371 (2001).
[40] P. A. Temple and C. Hathaway, Phys. Rev. B **7**, 3685 (1973).
[41] S. W. Lovesey, *Theory of Neutron Scattering from Condensed Matter* (Clarendon Press, Oxford, UK, 1984), Vol. 1.
[42] G. Kothleitner, M. J. Neish, N. R. Lugg, S. D. Findlay, W. Grogger, F. Hofer, and L. J. Allen, Phys. Rev. Lett. **112**, 085501 (2014).